Fast Uncertainty Quantification in Low Frequency Electromagnetic Problems by an Integral Equation Method Based on Hierarchical Matrix Compression

RICCARDO TORCHIO[ID][1,2], **LORENZO CODECASA**[ID][3], **(Member, IEEE),**
LUCA DI RIENZO[ID][3], **(Senior Member, IEEE), AND FEDERICO MORO**[ID][1], **(Member, IEEE)**

[1]Dipartimento di Ingegneria Industriale, Università degli Studi di Padova, 35131 Padova, Italy
[2]Univ. Grenoble Alpes, CNRS, Grenoble INP, G2Elab, 38000 Grenoble, France
[3]Dipartimento di Elettronica, Informazione e Bioingegneria, Politecnico di Milano, 20133 Milan, Italy

Corresponding author: Riccardo Torchio (riccardo.torchio@studenti.unipd.it)

ABSTRACT A parametric model order reduction method combined with a polynomial spectral approximation is applied for the first time to a Volume Integral Equation method accelerated by a low–rank matrix compression technique. Such an approach allows for drastically reducing the computational cost required by uncertainty quantifications in electromagnetic problems. Moreover, the proposed numerical tool can be adopted for computing stochastic information (e.g. mean, variance, probability density function) of any electromagnetic quantity of interest, in order to test the reliability of industrial devices with uncertainties on the material parameters. Conductive, dielectric, and magnetic media which exhibit uncorrelated and correlated random material parameters are considered by the proposed method.

INDEX TERMS Uncertainty quantification, integral equation method, parametric model order reduction, spectral approximation, electromagnetics, low–rank approximation, hierarchical matrices.

I. INTRODUCTION

In many electromagnetic (EM) applications the values of the material parameters are affected by unavoidable uncertainties [1], [2]. Moreover, conductivity, permittivity, and permeability of media are often strongly influenced by technological uncertainties and external uncontrolled phenomena, such as temperature, pressure, humidity, and other environmental quantities [3]. If not taken into account during the design stage, uncertainties on material parameters may significantly affect the reliability of devices, leading to a wrong evaluation of the system performances and the production of low–quality components [1].

Whenever the interest is the extraction of stochastic information (e.g. mean, variance, correlation) of some quantity of interest coming from the aleatory uncertainty in the input material parameters, the traditional Monte Carlo (MC) method can be adopted. However, even considering its

generality, MC requires to solve several deterministic problems (usually not less than 10,000), often resulting in a prohibitive computational effort.

To avoid this problem, many different techniques have been proposed in the literature, e.g. [1], [4], [5]. Most of them are based on the polynomial chaos expansion (PCE) [6], [7], which unfortunately does not allow for easily considering correlated random variables. The PCE technique has already been successfully applied to differential methods [8] and the Finite Integration Technique (FIT) method for magnetostatic [9], eddy-current [10], and electrokinetic [11] problems. Moreover, in [12], PCE has been successfully applied to an Integral Equation (IE) approach [13] based on the unstructured Partial Element Equivalent Circuit (PEEC) method [14], [15]. However, when the intrusive PCE in [12] is applied to IE methods, the computational cost and the memory requirement for the storage of dense matrices rapidly grow with the number of aleatory parameters. In this regard, low–rank compression techniques could be adopted to compress dense integral equation matrices and thus reduce the

---

The associate editor coordinating the review of this manuscript and approving it for publication was Nagarajan Raghavan[ID].

computational cost [16]. Unfortunately, the application of PCE to IE methods modifies the structure of the final system of equations which exhibits a complex pattern with both dense and sparse matrix blocks. Thus, the coupling of PCE–IE methods with low–rank matrix compression results numerically tricky.

Recently, in [17], an interesting and efficient alternative to the PCE technique, which allows for both uncorrelated and correlated material parameters, has been proposed for electrokinetic problems based on FIT method. This approach is based on Parametric Model Order Reduction (PMOR) [18], [19] and spectral approximation and it allows for drastically reducing the computational cost of uncertainty quantifications when random material parameters are considered.

Following [17], the idea behind the proposed numerical approach is to combine the well–known advantages of PMOR with the efficiency of spectral approximation technique in the context of VIE method coupled with low–rank approximation. In this paper, the numerical approach presented in [17] is sped up and applied for the first time to a Volume Integral Equation (VIE) method [20], [21]. In the presented VIE formulation, full Maxwell's equations are considered and conductive, dielectric, and magnetic media are included in the simulations. Moreover, unlike the PCE–PEEC method in [12], the proposed numerical approach can be easily combined with low–rank compression techniques. In this regard, the highly optimized $\mathcal{H}$LIBPro library [22] based on Hierarchical ($\mathcal{H}$) matrix representation [23] and Adaptive Cross Approximations (ACA) [24] is adopted, significantly reducing the computation time and memory required by VIE method [16]. For the sake of simplicity, in this paper the analysis is restricted to frequency values which allow neglecting the time delay effects on the propagation of the EM field, without falling back into the well–known numerical issues of VIE methods (see, e.g., [25], [26]).

The aim of this work is to provide a fast numerical tool for uncertainty quantification when media exhibit both uncorrelated and correlated random parameters. Thanks to the well–known advantages of VIE methods, which avoid the air discretization, the proposed approach can be efficiently applied for the study of devices surrounded by large air domains and/or with small air gaps, e.g. integrated circuit, electronic components, filters, etc. [14].

The computational cost required by the proposed approach is headed by the solution of only *few* deterministic VIE problems that, thanks to the use of low–rank approximation, can be significantly reduced. Moreover, thanks to the features of the proposed VIE formulation, the dense integral equation *coupling* matrices must be evaluated only once in compressed $\mathcal{H}$–form, whereas the sparse *material* matrices must be only updated. This leads to a very fast and efficient method where the time required for the assembly of the matrices and the dimension of the system to be solved is the same of a deterministic problem. Both 3–D and axisymmetric EM problems with a (relatively) high number of random material

parameters can be considered by the algorithm and the obtained results demonstrate the efficiency and accuracy of the proposed method. As shown in the numerical studies, the EM media can exhibit complex material quantities, where the real and the imaginary parts are considered as two potentially independent aleatory variables.

Numerical cases show that a very small dimension of the reduced order model is sufficient to attain very high accuracy. Indeed, with respect to [17] (where PMOR applied to FIT for an electrokinetic problem with only three parameters produces a reduced order model of dimension 20), the numerical results of this paper suggest that a reduced order model of much smaller dimension is needed when PMOR is applied to VIE. Moreover, the exponential convergence of the spectral approximation discussed in [7] is here observed.

The main outcomes of the implemented algorithm consist of: 1) a reduced order model of the parametric problem (section II-B) and, 2) a spectral expansion of any quantity derived from the unknowns of the EM problem (section III-B). Unlike approaches in the literature based on PCE, e.g. [12], the stochastic analysis can be carried out by assuming different probability distributions between the material parameters and correlation can be considered as well. Indeed, once obtained the spectral expansion of the quantity of interest, different stochastic analysis can be carried out without the need of re–running the algorithm.

Unlike [17], where the reduced order model is constructed through a greedy algorithm and a dense grid is adopted, in this paper a random selection strategy is used instead, thus avoiding the well–known problem of the *curse of dimensionality* during the construction of the reduced order model. Furthermore, the use of a random–based approach allows for improving the robustness of the PMOR algorithm, also avoiding stagnation problems [27]. Unlike [17], sparse grids are also successfully adopted for the spectral expansion, therefore mitigating the problem of the curse of dimensionality and significantly accelerating the algorithm. Thus, as shown in section IV where a problem with ten random material parameters is solved in few minutes only, the proposed numerical tool can be efficiently applied with some tens (e.g. 20-30) of random parameters.

The rest of the paper is organized as follows. In section II, the deterministic VIE formulation based on [28] is shortly presented. Then, the structure of the parametric problem is described. In section III, the stochastic method is then presented and subdivided in three parts. First, in section III-A, a PMOR algorithm which drastically reduces the dimension of the parametric problem is presented and widely discussed. In section III-B, a spectral approximation is applied to describe the relationships between the (aleatory) material parameters and the quantities of interest derived from the unknowns of the parametric VIE problem. Then, in section III-C, an MC simulation is finally applied to the spectral approximation with a negligible computational cost. In section IV, with the aim of validating and showing the computational performances of the proposed approach,

the analytical test case of a multi–shell dielectric sphere is considered. Finally, the model of the induction cookware presented in [29] is analyzed by the Stochastic–PMOR–VIE to show the performances of the method when applied to problems of industrial interest.

II. DETERMINISTIC VOLUME INTEGRAL EQUATION METHOD

In this paper, the deterministic VIE formulation proposed in [28], where the PEEC method is formulated in the framework of VIE, is considered. For the sake of clarity, the key points of [28] are here shortly reported.

A. VOLUME INTEGRAL EQUATION METHOD

Conductive, dielectric, and magnetic media are considered in the formulation. As it is customary, the term *dielectric* and *magnetic* specify media with permittivity and permeability different from those of vacuum, respectively. Moreover, the *electric* domain Ω_e (i.e. the union of the conductive and the dielectric regions) and the magnetic domain Ω_m are introduced together with the definitions of their boundaries, $\Gamma_e = \partial\Omega_e$ and $\Gamma_m = \partial\Omega_m$. Linear media which exhibit inhomogeneous and anisotropic properties can be considered as well. The whole EM problem is ruled by the following equations

$$\mathbf{E}(\mathbf{r}) = -i\omega\mathbf{A}_e(\mathbf{r}) - \nabla\varphi_e(\mathbf{r}) - \frac{1}{\varepsilon_0}\nabla \times \mathbf{A}_m(\mathbf{r}) + \mathbf{E}_{ext}(\mathbf{r}), \tag{1}$$

$$\mathbf{H}(\mathbf{r}) = -i\omega\mathbf{A}_m(\mathbf{r}) - \nabla\varphi_m(\mathbf{r}) + \frac{1}{\mu_0}\nabla \times \mathbf{A}_e(\mathbf{r}) + \mathbf{H}_{ext}(\mathbf{r}), \tag{2}$$

where $\mathbf{E}$ is the electric field, $\mathbf{H}$ is the magnetic field, $\mathbf{A}_e$ and $\mathbf{A}_m$ are the vector potentials, and φ_e and φ_m are the scalar electric and magnetic potentials introduced in [28]. The angular frequency is ω, i is the imaginary unit, $\mathbf{r}$ is the field point, and ε_0 and μ_0 are the vacuum permittivity and permeability, respectively. $\mathbf{E}_{ext}$ and $\mathbf{H}_{ext}$ are the incident electric and magnetic fields, respectively. Equations (1) and (2) are complemented by constitutive relationships

$$\mathbf{E}(\mathbf{r}) = \rho_e(\mathbf{r})\mathbf{J}_e(\mathbf{r}), \quad \mathbf{r} \in \Omega_e, \tag{3}$$

$$\mathbf{H}(\mathbf{r}) = \rho_m(\mathbf{r})\mathbf{J}_m(\mathbf{r}), \quad \mathbf{r} \in \Omega_m, \tag{4}$$

where $\mathbf{J}_e$ and $\mathbf{J}_m$ are the *electric* and *magnetic* current density vectors, respectively, whereas ρ_e and ρ_m are the *equivalent electric* and *magnetic resistivity*, defined as

$$\rho_e(\mathbf{r}) = \frac{1}{\sigma(\mathbf{r}) + i\omega\varepsilon_0(\varepsilon_r(\mathbf{r}) - 1)}, \quad \mathbf{r} \in \Omega_e, \tag{5}$$

$$\rho_m(\mathbf{r}) = \frac{1}{i\omega\mu_0(\mu_r(\mathbf{r}) - 1)}, \quad \mathbf{r} \in \Omega_m, \tag{6}$$

where σ is the electric conductivity, ε_r is the relative permittivity, and μ_r is the relative permeability.

Following [28], vector and scalar potentials in (1) and (2) are given by their classical integral expressions which depend

on $\mathbf{J}_e$ and $\mathbf{J}_m$. Then, (1)–(4) are combined together, $\mathbf{J}_e$ and $\mathbf{J}_m$ are expanded by means of Whitney face shape functions, and the resulting equations are tested by Galerkin approach (i.e. by using the same Whitney face shape functions as test functions). This results in

$$(\mathbf{R}_e + i\omega\mathbf{L}_e + \frac{1}{i\omega}\mathbf{D}_{\Omega_e}^{aT}\mathbf{P}_e\mathbf{D}_{\Omega_e}^{a})\mathbf{j}_e + \mathbf{Z}_{12}\mathbf{j}_m = \mathbf{e}_0, \tag{7}$$

$$(\mathbf{R}_m + i\omega\mathbf{L}_m + \frac{1}{i\omega}\mathbf{D}_{\Omega_m}^{aT}\mathbf{P}_m\mathbf{D}_{\Omega_m}^{a})\mathbf{j}_m + \mathbf{Z}_{21}\mathbf{j}_e = \mathbf{h}_0, \tag{8}$$

where $\mathbf{j}_e = (j_{e_k})$ and $\mathbf{j}_m = (j_{m_k})$ are the arrays of DoFs corresponding to the fluxes of $\mathbf{J}_e$ and $\mathbf{J}_m$ through the faces of the mesh, respectively, $\mathbf{e}_0 = (e_{0_k})$ and $\mathbf{h}_0 = (h_{0_k})$ are the DoFs corresponding to $\mathbf{E}_{ext}$ and $\mathbf{H}_{ext}$, respectively. Sparse resistance matrices $\mathbf{R}_e$ and $\mathbf{R}_m$ are the only matrices that depend on material parameters. Their coefficients are:

$$R_{e_{hk}} = \int_{\Omega_e} \rho_e(\mathbf{r})\mathbf{w}_h(\mathbf{r}) \cdot \mathbf{w}_k(\mathbf{r})d\Omega, \tag{9}$$

$$R_{m_{hk}} = \int_{\Omega_m} \rho_m(\mathbf{r})\mathbf{w}_h(\mathbf{r}) \cdot \mathbf{w}_k(\mathbf{r})d\Omega, \tag{10}$$

where $\mathbf{w}_k$ is the face shape function related to the kth face of the mesh of Ω_e or Ω_m. Other matrices in (7) and (8) are defined in [28] and are with coefficients not depending on material parameters.

Equations (7) and (8) are obtained from the discretization of the integral continuum equations (1) and (2), where $\mathbf{j}_e$ and $\mathbf{j}_m$ have been chosen as unknowns. However, different choices of the unknowns are possible, as that ones described in [30] or [31], which lead to alternative VIE methods [25], [26]. Moreover, depending on the kind of EM problem to be solved, many techniques can be applied to improve the numerical properties of the final system [30], avoid the numerical issues common to IE methods (e.g. breakdown in frequency) [32], [33], and strongly enforce the div–free condition of the current density [34]. For the sake of simplicity, these methods (which mostly require a *change of basis* and a projection of (7) and (8) into a new set of equations [34]) are not discussed here. However, any numerical technique which preserves the structure of (7) and (8) can be applied without compromising the following discussion.

B. PARAMETRIC PROBLEM

The deterministic VIE problem is now transformed into a parametric problem. Let $\Omega_a = \Omega_e \cup \Omega_m$ be the active domain consisting of K sub–domains Ω_k, with $k = 1, \cdots, K$, where the electric and magnetic resistivity are piecewise constant functions equal to $\bar{\rho}_{e_k}$ and $\bar{\rho}_{m_k}$ in each sub–region Ω_k , i.e. $\rho_e(\mathbf{r}) = \bar{\rho}_{e_k}$ and $\rho_m(\mathbf{r}) = \bar{\rho}_{m_k}$ with $\mathbf{r} \in \Omega_k$. Thus, (7) and (8) can be recast into a unique matrix system

$$[\mathbf{R} + \mathbf{U}]\mathbf{x} = \mathbf{b}, \tag{11}$$

where $\mathbf{U}$, $\mathbf{x}$, and $\mathbf{b}$ are defined independently of the subdivision of Ω_a:

$$\mathbf{x} = \begin{bmatrix} \mathbf{j}_e \\ \mathbf{j}_m \end{bmatrix}, \quad \mathbf{b} = \begin{bmatrix} \mathbf{e}_0 \\ \mathbf{h}_0 \end{bmatrix}, \tag{12}$$

$$\mathbf{U} = \begin{bmatrix} i\omega\mathbf{L}_e + \dfrac{1}{i\omega}\mathbf{D}^{aT}_{\Omega_e}\mathbf{P}_e\mathbf{D}^{a}_{\Omega_e} & \mathbf{Z}_{12} \\ \mathbf{Z}_{21} & i\omega\mathbf{L}_m + \dfrac{1}{i\omega}\mathbf{D}^{aT}_{\Omega_m}\mathbf{P}_m\mathbf{D}^{a}_{\Omega_m} \end{bmatrix}. \tag{13}$$

The resistance matrix $\mathbf{R}$ is given by

$$\mathbf{R} = \sum_{k=1}^{K} \bar{\rho}_k \mathbf{R}_k, \tag{14}$$

with

$$\bar{\rho}_k \mathbf{R}_k = \begin{bmatrix} \bar{\rho}_{e_k}\mathbf{R}_{e_k} & \mathbf{0} \\ \mathbf{0} & \bar{\rho}_{m_k}\mathbf{R}_{m_k} \end{bmatrix}, \tag{15}$$

where $\mathbf{R}_{e_k}$ and $\mathbf{R}_{m_k}$ are defined as in (9) and (10) by setting a value of the electric and magnetic resistivity equal to 1 in the kth sub–region and 0 elsewhere. For the sake of simplicity and with a slight abuse of notation, the *general* resistivity $\bar{\rho}_k$ equal to $\bar{\rho}_{e_k}$ in Ω_e and to $\bar{\rho}_{m_k}$ in Ω_m has been introduced in (14) and (15).

Equation (11) can now be transformed into a *parametric* problem. Each resistivity value $\bar{\rho}_{e_k}$ and $\bar{\rho}_{m_k}$ (with $k = 1, \cdots, K$) can be considered as a function of a small number Q of parameters $\xi_1, \cdots, \xi_Q$ stored in the vector array $\boldsymbol{\xi}$, i.e. $\bar{\rho}_k = \bar{\rho}_k(\boldsymbol{\xi})$. Each parameter ξ_k, with $k = 1, \cdots, Q$, varies in the set $[-1, 1]$. Thus $\boldsymbol{\xi}$ varies in the set $\boldsymbol{\Xi} = [-1, 1]^Q$, i.e. the Q–dimensional master hypercube. Therefore, the parametric EM problem is ruled by

$$\left[\sum_{k=1}^{K} \bar{\rho}_k(\boldsymbol{\xi})\mathbf{R}_k + \mathbf{U} \right] \mathbf{x}(\boldsymbol{\xi}) = \mathbf{b}. \tag{16}$$

If $\bar{\rho}_k$ are modeled with a given Probability Density Function (PDF), an MC method can be applied to extract stochastic information of some quantity of interest. Therefore, (16) must be solved for each MC sample. Thus, due to the slow convergence of the MC approach, this method usually results in a prohibitive computation time. Moreover, if the assumption on the PDF of the resistivity changes, the MC simulation must be performed again. In section III, an alternative method which drastically reduces the computation time required by the stochastic analysis is proposed.

As shown by many works in the literature [16], [35], [36], low–rank compression techniques can be efficiently applied to integral equation methods. Indeed, although fully populated, matrix $\mathbf{U}$ contains low–rank off-diagonal blocks that make $\mathbf{U}$ compressible in some sense. In this regard, many toolboxes based on different kinds of low–rank matrix representation are available, e.g. Hierarchical Off–Diagonal Low–Rank (HODLR) [37], Hierarchical–Semi–Separable (HSS) [38]–[41], and Hierarchical $\mathcal{H}$ and $\mathcal{H}^2$ [22] format. Such methods based on hierarchical matrices allows for representing $\mathbf{U}$ in a suitable data–sparse format that stores its rank–deficient blocks by computing a reduced number of entries only. It should be noted, however, that in (16) a sparse matrix is summed up a dense matrix, therefore the chosen low–rank library must support the representation of

sparse matrices in hierarchical format and the matrix–matrix addition in hierarchical–matrix arithmetic. In this work, the highly optimized $\mathcal{H}$LIBPro library based on $\mathcal{H}$–matrix representation (and $\mathcal{H}^2$–matrices for the construction of cluster bases) is adopted [22]. However, other choices are also possible [42]–[44].

III. STOCHASTIC VIE METHOD

The key idea is not to completely avoid the use of MC, which, beyond its slow convergence, is a general and robust method. Instead, the goal is to drastically reduce the computational effort of the problem and finally apply MC to a simple equation. At this purpose, a parametric model order reduction is first applied to (16) and then a spectral expansion is applied to the reduced order model. Finally, MC is applied to the spectral expansion with a negligible computational effort. In the following, these three steps are described.

A. PARAMETRIC MODEL ORDER REDUCTION

The *reduced parametric model* of (16) is constructed by using an iterative approach based on Parametric Model–Order Reduction [18], [19]. In this paper, an enhanced version of the algorithm proposed in [17] is adopted. In [17], a greedy algorithm [45] and a (dense) grid obtained as the Cartesian product of Gaussian Points of Legendre polynomials were adopted for the construction of the reduced order model, incurring in the curse of dimensionality problem. In this work, a random–based method for the construction of the reduced order model is used instead, thus avoiding the problem of the curse of dimensionality and significantly accelerating the algorithm without loosing accuracy, as shown in section IV. Moreover, the use of a random–based approach allows for improving the robustness of the PMOR algorithm, avoiding stagnation problems [27]. Such *accelerated* procedure is reported in Algorithm 1 and thoroughly discussed in the following.

According to the PMOR Algorithm 1, at step 0, the projection matrix $\mathbf{V}_0$ is initialized to the empty set and the index c, counting the number of iterations of the algorithm, is initialized to 1.

Then, at step 1, the parametric problem ruled by (16) is solved in $\mathcal{H}$–arithmetic for a given choice of $\boldsymbol{\xi}$, which is initialized to zero, i.e. $\boldsymbol{\xi} = \mathbf{0}$, at the beginning of the algorithm.

At step 2, the projection matrix $\mathbf{V}_c$ is evaluated by applying a Gram-Schmidt orthogonalization (GSO) to the set of vectors made of $\mathbf{x}(\boldsymbol{\xi})$ (i.e. the solution of the parametric problem obtained at step 1) and columns of $\mathbf{V}_{c-1}$:

$$\mathbf{V}_c = \text{GSO}([\mathbf{V}_{c-1}, \mathbf{x}(\boldsymbol{\xi})]). \tag{17}$$

Columns of $\mathbf{V}_c$ are orthonormal basis vectors of the space spanned by all the solutions obtained at step 1. Thus, $\mathbf{V}_c$ is a $N_x \times c$ orthonormal matrix, where N_x is the dimension of the parametric problem (i.e. the dimension of $\mathbf{x}(\boldsymbol{\xi})$).

At step 3, the parametric reduced model $\mathcal{M}_c$ is finally constructed by projecting (16) onto the space spanned by the

---

Algorithm 1 PMOR Algorithm

Input: Matrices $\mathbf{U}$ and $\mathbf{R}_k$ in $\mathcal{H}$–format and the functions $\bar{\rho}_k(\boldsymbol{\xi})$, (with $k = 1, \cdots, K$)

Set $\mathbf{V}_0 = \emptyset$ //{0}
Set $c = 1$
Set $\boldsymbol{\xi} = \mathbf{0}$
Set $r = +\infty$
Set N_{rand} (e.g. $N_{rand} = 10$)
Set a desired value of η (e.g. $\eta = 10^{-3}$)
while $r > \eta$ **do**
   Find the solution $\mathbf{x}(\boldsymbol{\xi})$ of (16) in $\mathcal{H}$–arithmetic:
$$\mathbf{x}(\boldsymbol{\xi}) = \left[\sum_{k=1}^{K} \bar{\rho}_k(\boldsymbol{\xi})\mathbf{R}_k + \mathbf{U} \right] \backslash \mathbf{b}. \qquad //\{1\}$$
   Update the orthonormal basis of dimension $\mathcal{M}_c$:
$$\mathbf{V}_c = \text{GSO}([\mathbf{V}_{c-1}, \mathbf{x}(\boldsymbol{\xi})]) \qquad //\{2\}$$
   Generate the reduced order model $\mathcal{M}_c$ (in $\mathcal{H}$–arithmetic):
$$\hat{\mathbf{U}}_c = \mathbf{V}_c^T \mathbf{U} \mathbf{V}_c,$$
$$\hat{\mathbf{R}}_{c_k} = \mathbf{V}_c^T \mathbf{R}_k \mathbf{V}_c, \text{ with } k = 1, \cdots, K \quad //\{3\}$$
   Generate N_{rand} random values of $\boldsymbol{\xi} \in \Xi$ //{4}
   for $h = 1, \cdots, N_{rand}$ (*parallel*) **do**
      Select the hth random point $\boldsymbol{\zeta}_h$
      Find the solution $\hat{\mathbf{x}}(\boldsymbol{\zeta}_h)$ of the reduced order problem (18) and then evaluate $\tilde{\mathbf{x}}(\boldsymbol{\zeta}_h) = \mathbf{V}_c\hat{\mathbf{x}}(\boldsymbol{\zeta}_h)$ //{5}
      Evaluate the residual:
$$r_h' = \left\| \left[\sum_{k=1}^{K} \bar{\rho}_k(\boldsymbol{\zeta}_h)\mathbf{R}_k + \mathbf{U} \right] \tilde{\mathbf{x}}(\boldsymbol{\zeta}_h) - \mathbf{b} \right\| / \|\mathbf{b}\|$$
$$//\{6\}$$
   end for
   Find $M \in [1, \cdots, N_{rand}]$ such that
$$r_M' = \max(r_h', \text{with } h = 1, \cdots, N_{rand})$$
   Set $r = r_M'$
   Set $\boldsymbol{\xi} = \boldsymbol{\zeta}_M$ //{7}
   if $r > \eta$ **then**
      Set $c = c + 1$
   end if
end while
Output: Reduced order model $\mathcal{M}_c$ consisting of $\hat{\mathbf{U}}_c$ and $\hat{\mathbf{R}}_{k_c}$, with $k = 1, \cdots, K$, and the projection matrix $\mathbf{V}_c$

---

columns of $\mathbf{V}_c$, i.e.

$$\left[\sum_{k=1}^{K} \bar{\rho}_k(\boldsymbol{\xi})\hat{\mathbf{R}}_{c_k} + \hat{\mathbf{U}}_c \right] \hat{\mathbf{x}}(\boldsymbol{\xi}) = \hat{\mathbf{b}}_c, \qquad (18)$$

where:

$$\hat{\mathbf{b}}_c = \mathbf{V}_c^T \mathbf{b}, \qquad (19)$$

$$\hat{\mathbf{U}}_c = \mathbf{V}_c^T \mathbf{U} \mathbf{V}_c, \qquad (20)$$

$$\hat{\mathbf{R}}_{c_k} = \mathbf{V}_c^T \mathbf{R}_k \mathbf{V}_c. \qquad (21)$$

$\hat{\mathbf{U}}_c$ and $\hat{\mathbf{R}}_{c_k}$ (with $k = 1, \cdots, K$) are square matrices of dimension $c \times c$, $\hat{\mathbf{b}}$ is a vector array of dimension c, and $\hat{\mathbf{x}}(\boldsymbol{\xi})$ is the solution of $\mathcal{M}_c$ for a given choice of $\boldsymbol{\xi}$.

It is worth noting that $\hat{\mathbf{U}}_c$ and $\hat{\mathbf{R}}_{c_k}$ are usual uncompressed matrices (of small dimension), whereas $\mathbf{U}$ and $\mathbf{R}_k$ are compressed $\mathcal{H}$–matrices. Thus, matrix–matrix multiplication in (20) and (21) must be performed in $\mathcal{H}$–arithmetic. Therefore, the chosen low–rank library must support $\mathcal{H}$ matrix–vector multiplication, which is indeed supported by $\mathcal{H}$LIBPro.

A parametric reduced order model $\mathcal{M}_c$ of dimension c is now constructed. This model of reduced dimension allows for obtaining an approximate solution of the original parametric problem (16). Indeed, when $\hat{\mathbf{x}}(\boldsymbol{\xi})$ is obtained by solving (18), an approximate solution of (16), i.e. $\mathbf{x}(\boldsymbol{\xi}) \simeq \tilde{\mathbf{x}}(\boldsymbol{\xi})$, is given by

$$\tilde{\mathbf{x}}(\boldsymbol{\xi}) = \mathbf{V}_c\hat{\mathbf{x}}(\boldsymbol{\xi}). \qquad (22)$$

In the following steps of the algorithm, $\mathcal{M}_c$ is tested against a selected number N_{rand} (e.g. $N_{rand} = 10$) of random values of $\boldsymbol{\zeta} \in \Xi$ to check if the reduced model actually provides an accurate approximation of the original parametric problem (16).

Thus, at step 4, random points $\boldsymbol{\zeta}_h \in \Xi$ with $\boldsymbol{\zeta}_h = 1, \cdots, N_{rand}$ are generated and, at step 5, (18) is solved for each value of $\boldsymbol{\zeta}_h$, and the approximate solutions $\tilde{\mathbf{x}}(\boldsymbol{\zeta}_h)$ are evaluated according to (22).

Then, at step 6, the accuracy of each approximate solution $\tilde{\mathbf{x}}(\boldsymbol{\zeta}_h)$, with $h = 1, \cdots, N_{rand}$, is tested by evaluating the related hth residual (in $\mathcal{H}$–arithmetic) as

$$r_h' = \frac{\left\| \left[\sum_{k=1}^{K} \bar{\rho}_k(\boldsymbol{\zeta}_h)\mathbf{R}_k + \mathbf{U} \right] \tilde{\mathbf{x}}(\boldsymbol{\zeta}_h) - \mathbf{b} \right\|}{\|\mathbf{b}\|}. \qquad (23)$$

If for each point $\boldsymbol{\zeta}_h$, the residual r_h' is smaller than the required tolerance η, then the algorithm stops and the reduced order model $\mathcal{M}_c$ of dimension c is obtained. Instead, if r_h' is greater than η for some points of $\boldsymbol{\zeta}_h$, the one which maximizes the value of the residual is chosen as the next candidate of a further iteration of the algorithm.

Thus, at step 7, $\boldsymbol{\xi}$ is set equal to the random point $\boldsymbol{\zeta}_M$ which maximizes the residual r. Then, if $r > \eta$, the value of the counter c is updated (i.e. $c = c + 1$) and the algorithm restarts from step 1. At each iteration of Algorithm 1, the reduced order model is not re–constructed from scratch. Instead, only the *new information* obtained from the solution of (16) for a new selected random point is added to $\mathcal{M}_{c-1}$, resulting into $\mathcal{M}_c$. It is worth noting that, thanks to the Gram-Schmidt orthogonalization, only the orthogonal components of the new solution (i.e. the new informations) are added to $\mathcal{M}_c$.

The dimension c of the reduced order model $\mathcal{M}_c$ is generally much smaller than N_x (i.e. the dimension of the original parametric problem). Thus, in the context of stochastic analysis, an MC approach can now be performed by solving the reduced order model $\mathcal{M}_c$ for each sample $\boldsymbol{\xi}_h$, with $h = 1, \cdots, N_{MC}$ and N_{MC} is the number of MC samples. The adoption of a PMOR strategy for uncertainty quantifications has been already proposed for different kinds of problems [46]–[49]. However, since the MC method exhibits a $\mathcal{O}(1/\sqrt{N_{MC}})$ convergence rate, when the stochastic

analysis requires a high accuracy, the value of N_{MC} grows significantly, and therefore also the computation time, using the parametric reduced-order model.

In section III-B, with the aim of further reducing the computational cost required by the stochastic analysis, a spectral approximation is applied to the reduced order model $\mathcal{M}_c$.

B. SPECTRAL APPROXIMATION

Let us now assume that a given quantity of interest, $w(\boldsymbol{\xi})$, is obtained as a function of $\mathbf{x}(\boldsymbol{\xi})$ (i.e. the solution of the parametric problem (16)), as

$$w(\boldsymbol{\xi}) = \mathcal{F}(\mathbf{x}(\boldsymbol{\xi})). \tag{24}$$

For instance, $w(\boldsymbol{\xi})$ can be the electric or the magnetic field components in a given target point, the joule losses, the equivalent impedance of a device (which is the case of the induction cookware considered in section IV-B), etc. All these quantities can be directly obtained from $\mathbf{x}(\boldsymbol{\xi})$ by applying a proper operator here defined as the continuous function $\mathcal{F}(\cdot)$.

A spectral approximation can be then applied and reads [7]

$$w(\boldsymbol{\xi}) = \sum_{|\boldsymbol{\alpha}| \leq P} w_{\boldsymbol{\alpha}} \boldsymbol{\psi}_{\boldsymbol{\alpha}}(\boldsymbol{\xi}), \tag{25}$$

where $w_{\boldsymbol{\alpha}}$ is the projection of $w(\boldsymbol{\xi})$ onto $\boldsymbol{\psi}_{\boldsymbol{\alpha}}(\boldsymbol{\xi})$, i.e.

$$w_{\boldsymbol{\alpha}} = \int_{\Xi} w(\boldsymbol{\xi}) \boldsymbol{\psi}_{\boldsymbol{\alpha}}(\boldsymbol{\xi}) d\boldsymbol{\xi}. \tag{26}$$

In (26), $\boldsymbol{\alpha} = (\alpha_1, \cdots, \alpha_Q)$ is a multi–index of Q elements with $|\boldsymbol{\alpha}| = \alpha_1 + \cdots + \alpha_Q$, and

$$\boldsymbol{\psi}_{\boldsymbol{\alpha}}(\boldsymbol{\xi}) = \psi_{\alpha_1}(\xi_1)\psi_{\alpha_1}(\xi_2) \cdots \psi_{\alpha_Q}(\xi_{Q-1})\psi_{\alpha_Q}(\xi_Q), \tag{27}$$

in which ψ_p, with $p = 0, \cdots, P$, are the first $P + 1$ Legendre polynomials defined in $[-1, 1]$. Functions $\boldsymbol{\psi}_{\boldsymbol{\alpha}}$, with $|\boldsymbol{\alpha}| \leq P$, form a basis of all polynomials in Q variables and of degree smaller or equal to P, with dimension

$$N_{pol} = \binom{P + Q}{P}. \tag{28}$$

Starting from the reduced order model $\mathcal{M}_c$ (i.e. the output of Algorithm 1), the spectral approximation of $w(\boldsymbol{\xi})$ shown in (25) can be obtained with the non–intrusive method described in Algorithm 2.

According to Algorithm 2, at step 8, a Q–dimensional grid defined as $\boldsymbol{\chi}$ is constructed. For the moment, this grid is assumed to be the Cartesian product of Q sets of P Gaussian points of Legendre polynomials resulting in $N_{\boldsymbol{\chi}} = P^Q$ grid points. However, as discussed in the following, other choices of $\boldsymbol{\chi}$ are possible. The points of the grid are indicated as $\boldsymbol{\zeta}_h$, with $h = 1, \cdots, N_{\boldsymbol{\chi}}$. At step 9, the reduced order model obtained as output of Algorithm 1 is solved for all the points of $\boldsymbol{\chi}$. Thus, for each solution $\hat{\mathbf{x}}(\boldsymbol{\zeta}_h)$, with $h = 1, \cdots, N_{\boldsymbol{\chi}}$, the approximate solution $\tilde{\mathbf{x}}(\boldsymbol{\zeta}_h)$ is obtained from (22). At step 10, according to (24), an approximation of $w_h(\boldsymbol{\zeta}_h)$ is obtained and then stored in the array $\mathbf{w} = (w_h)$, with $h = 1, \cdots, N_{\boldsymbol{\chi}}$.

Algorithm 2 Spectral Approximation Algorithm

Input: Reduced order model $\mathcal{M}_c$ consisting of $\hat{\mathbf{U}}_c$ and $\hat{\mathbf{R}}_{k_c}$, with $k = 1, \cdots, K$, and the projection matrix $\mathbf{V}_c$

Construct $\boldsymbol{\chi}$ // {8}

for $h = 1, \cdots, N_{\boldsymbol{\chi}}$ (*parallel*) **do**

    Extract the hth grid point $\boldsymbol{\zeta}_h$ of $\boldsymbol{\chi}$

    Find the solution $\hat{\mathbf{x}}(\boldsymbol{\zeta}_h)$ of the reduced order problem (18) and then evaluate $\tilde{\mathbf{x}}(\boldsymbol{\zeta}_h) = \mathbf{V}_c\hat{\mathbf{x}}(\boldsymbol{\zeta}_h)$ // {9}

    Evaluate the approximated quantity $w_h(\boldsymbol{\zeta}_h) \simeq \mathcal{F}(\tilde{\mathbf{x}}(\boldsymbol{\zeta}_h))$ // {10}

    Store w_h in the vector array $\mathbf{w} = (w_h)$

end for

for $|\boldsymbol{\alpha}| \leq P$ (*parallel*) **do**

    Set $w_{\boldsymbol{\alpha}} = 0$

    for $h = 1, \cdots, N_{\boldsymbol{\chi}}$

    do

        $w_{\boldsymbol{\alpha}} = w_{\boldsymbol{\alpha}} + w_h W_h \boldsymbol{\psi}_{\boldsymbol{\alpha}}(\boldsymbol{\zeta}_h)$ // {11}

    end for

end for

Output: Spectral approximation of $w(\boldsymbol{\xi})$

Finally, at step 11, the $\boldsymbol{\alpha}$th spectral projection of $w(\boldsymbol{\xi})$ is approximated by numerically integrating (26) with a Gaussian quadrature rule in the grid points of $\boldsymbol{\chi}$:

$$w_{\boldsymbol{\alpha}} = \sum_{h=1}^{N_{\boldsymbol{\chi}}} w_h W_h \boldsymbol{\psi}_{\boldsymbol{\alpha}}(\boldsymbol{\zeta}_h), \tag{29}$$

where W_h is the weight related to the hth Gauss point, with $h = 1, \cdots, N_{\boldsymbol{\chi}}$.

The two *for–loops* in Algorithm 2 (as well the one of Algorithm 1) can be executed in parallel by the workers of multi–core computers or clusters. However, due to the curse of dimensionality, the number of points of $\boldsymbol{\chi}$ (i.e. $N_{\boldsymbol{\chi}} = P^Q$) exponentially increases with the dimension Q. Therefore, the computation time required by the *for–loops* in Algorithm 2 significantly increases with Q, even with a parallelized *for–loop*. A (partial) solution to this problem consists in replacing the Gaussian grid $\boldsymbol{\chi}$ with a sparse grid $\boldsymbol{\chi}^*$ [7]. Sparse grids have been introduced as a computationally more efficient method of integrating multidimensional functions. The Gaussian grid $\boldsymbol{\chi}$ is obtained as a (complete) tensor product of Q sets of Gaussian points, whereas the sparse grid $\boldsymbol{\chi}^*$ is obtained as a much smaller subset of the tensor product. The sparse grid MATLAB® toolbox in [50] based on the Clenshaw-Curtis rule is used in the implementation. Different kinds of quadrature rules can however be used [51]. The number of points of the sparse grid for this rule is

$$N_{\boldsymbol{\chi}^*} \approx \frac{2^L Q^L}{L!}, \quad \text{with } Q \gg 1, \tag{30}$$

where L denotes the *level* of the sparse grid [7]. Moreover, unlike to the Gauss–Legendre points, the Clenshaw-Curtis points are mostly located on the boundary of the grid. In such

a way the spectral approximation explores the boundary of Ξ which usually holds *useful information* of the parametric problem.

C. MONTE CARLO ANALYSIS

The procedure described above is completely *deterministic*. Let us now assume that the interest is to quantify the uncertainty of w deriving from the uncertainty of the material parameters (i.e. $\bar{\rho}_k$, with $k = 1, \cdots, Q$). MC analysis can be efficiently carried out by using the spectral approximation of w. N_{MC} Monte Carlo samples ξ_h, with $h = 1, \cdots, N_{MC}$, are generated according to the Probability Density Function (PDF) of each hth parameter. Then, $w(\xi_h)$ is efficiently evaluated by using (25). Thus, even when N_{MC} is very large (e.g. $N_{MC} > 10^6$), the whole computational effort can be reasonably addressed. In this manner unprecedented levels of accuracy in the stochastic analysis when random variables are correlated can be achieved. Moreover, as discussed in [17], a further advantage of the proposed method is the completely independence on the PDF of the material quantities. Furthermore, the case of correlation between the material parameters can be considered as well.

Finally, a significant advantage over other methods proposed in the literature is that the spectral approximation of w can be adopted assuming different PDFs of the Q parameters without re–running Algorithm 1 and Algorithm 2.

IV. NUMERICAL RESULTS

The Stochastic–PMOR–VIE algorithm was implemented in MATLAB® and FORTRAN coupled with the C interface of $\mathcal{H}$LIBPro library. In this section, an analytical problem and a industrial test case are considered. Simulations were run on a Linux machine equipped with a Xeon E5-2643 v4 processor (dual 6-core/12-thread, @3.40 GHz) and 512 GB RAM.

A. MULTI–SHELL SPHERE

In order to validate and test the performance of the proposed method, the case of a dielectric multi–shell sphere consisting of 5 concentric shells is considered (Fig. 1). The external radius of the shields are 1 m, 0.8 m, 0.6 m, 0.4 m, and 0.2 m, respectively. The thickness of each layer is 0.1 m. The sphere is excited by an external plane wave $\mathbf{E}_{ext}(\mathbf{r}) = e^{-ik_0 z}\mathbf{u}_x$, where $k_0 = 2\pi f \sqrt{\frac{\varepsilon_0}{\mu_0}}$ and $f = 5$ MHz frequency.

The real and the imaginary part of the electric permittivity of each layer is considered to be an aleatory variable. Thus, the electric permittivity of the kth layer, with $k = 1, \cdots, 5$, is given by

$$\varepsilon_{r_k} = \Re(\varepsilon_{r_{m,k}}) + \xi_{2k-1}\Re(\Delta\varepsilon_{r_k}) + i\Big(\Im(\varepsilon_{r_{m,k}}) + \xi_{2k}\Im(\Delta\varepsilon_{r_k})\Big),$$
(31)

where the mean values and the variation ranges of the real and imaginary parts are given in Table 1. Thus, for this analytical case, the number of parameters is $Q = 10$ (i.e. the size of ξ). Two different cases are considered: 1) the real and the imaginary parts of the permittivity values are considered as
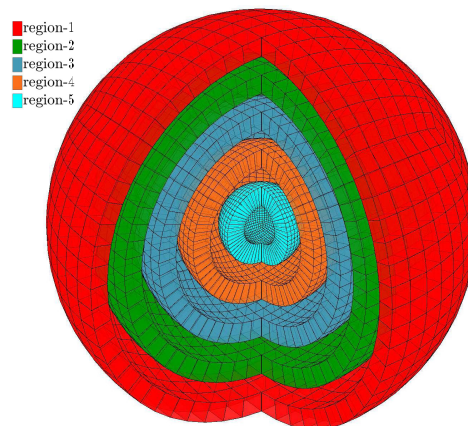

FIGURE 1. Slice view (3/4 of multi–shell sphere model).

TABLE 1. Permittivity values for any shell.

Region	$\Re(\varepsilon_{r_m})$	$\Im(\varepsilon_{r_m})$	$\Re(\Delta\varepsilon_r)$	$\Im(\Delta\varepsilon_r)$
1	25	−25	22	−22
2	15	−15	10	−10
3	20	−15	15	−14
4	17	−15	13	−13
5	20	−18	18	−16

10 statistically independent aleatory variables with uniform PDFs in the ranges defined by Table 1 (*uncorrelated* case); 2) the same uniform marginal PDFs are assumed for the 10 aleatory variables and a Gaussian copula with correlation matrix $\mathcal{C}$, with non–zero entries

$$\mathcal{C}(k, k) = 1, \quad \text{with } k = 1, \cdots, 10,$$
$$\mathcal{C}(1, 6) = \mathcal{C}(6, 1) = -0.7250,$$
$$\mathcal{C}(9, 10) = \mathcal{C}(10, 9) = -0.8023, \quad (32)$$

is introduced (*correlated* case) [52].

The spectral approximation procedure described in section III-B is applied to the active power losses generated in the dielectric shells. Thus, in this analytical case, the quantity of interest introduced in (24) is evaluated as

$$w(\xi) = \mathcal{F}(\mathbf{x}(\xi)) = \frac{1}{2}\Re\Big(\mathbf{x}(\xi)^T \mathbf{R}\mathbf{x}(\xi)\Big).$$

Different (approximated) sets of random samples of w consisting of $N_{MC} = 10,000$ values are extracted from the Stochastic–PMOR–VIE algorithm: sets F_{MC-c}, with $c = 2, \cdots, 13$, are obtained by directly applying the MC method on the reduced order model $\mathcal{M}_c$ (as described at the end of section III-A); sets F_{SP-c} are obtained by running an MC method on the spectral approximation (25) of order $P = 5$ starting from the reduced order model $\mathcal{M}_c$ with $c = 2, \cdots, 13$. Moreover, the *Reference* set F_{Ref} is obtained by running an MC method on the *Mie solution* of the problem implemented in the free MATLAB® tool available in [53].

Fig. 2 and Fig. 3 show the PDFs of w for the *uncorrelated* and *correlated* cases, respectively. Such PDFs are extracted from the sets of random samples described above. With the
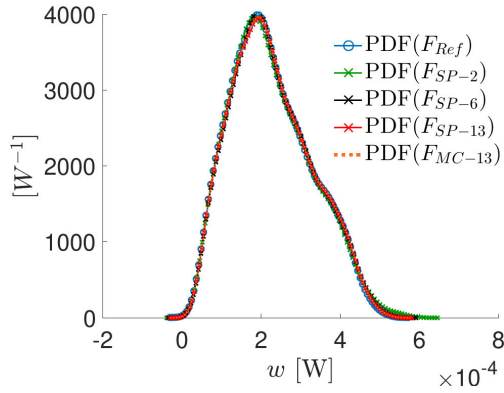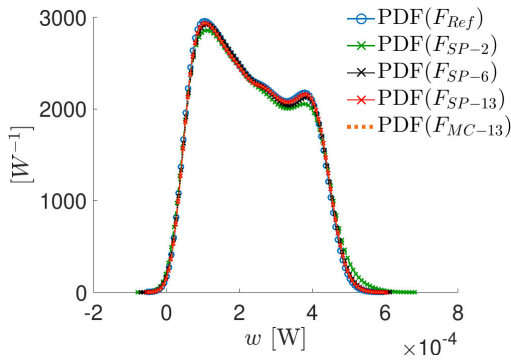
FIGURE 2. PDF of *w* for the uncorrelated case.

FIGURE 3. PDF of *w* for the correlated case.

FIGURE 4. PDF of *w* for the correlated case obtained from the spectral approximation for different sets of random samples with $N_{MC} = 10^2$, $10^3, \ldots, 10^7$.

FIGURE 5. (a) Residual *r* of Algorithm 1 for iterations $c = 2, \ldots, 13$ obtained from the proposed random and greedy PMOR methods. (b) Kolmogorov Smirnov statistic (distance) between the set F_{MC-c}, with $c = 2, \ldots, 13$, and the reference set F_{Ref} for the uncorrelated and correlated cases.

aim of allowing a fair comparison, the same set of N_{MC} samples is adopted for all the MC simulations (i.e. one set for the uncorrelated case, and another set based on the correlation matrix $\mathcal{C}$ for the correlated case). Fig. 2 and Fig. 3 show a very good agreement between the PDFs for both the correlated and uncorrelated case. Moreover, even if only two correlation coefficients have been introduced between the parameters, a significant difference between the uncorrelated and correlated cases can be noted.

Fig. 4 shows the PDFs of *w* for the correlated case obtained from the spectral approximation applied to $\mathcal{M}_{13}$ for different sets of random samples with $N_{MC} = 10^2, 10^3, \cdots, 10^7$. It can be seen that when high accuracy is required a large number of random samples N_{MC} is needed, which can be easily handled by the proposed procedure.

Fig. 5 (*a*) shows the convergence of Algorithm 1 proposed in this paper (random PMOR) and the convergence of the greedy method introduced in [17] (greedy PMOR). When tested against 10 random points $\boldsymbol{\xi}_h \in \Xi$, with $k = 1, \cdots, 10$, the reduced order model obtained from the random method and the one obtained from the greedy algorithm of [17] produce equivalent results (values differ less than 0.1% in the parametric solution and show the same accuracy when compared to the exact solution of (16)), demonstrating that the random approach does not affect the accuracy.
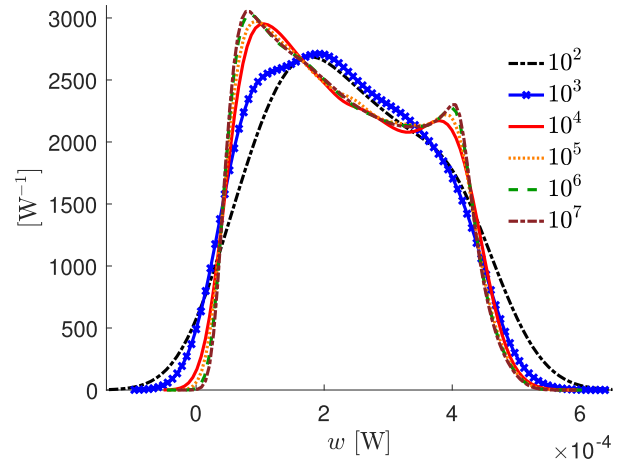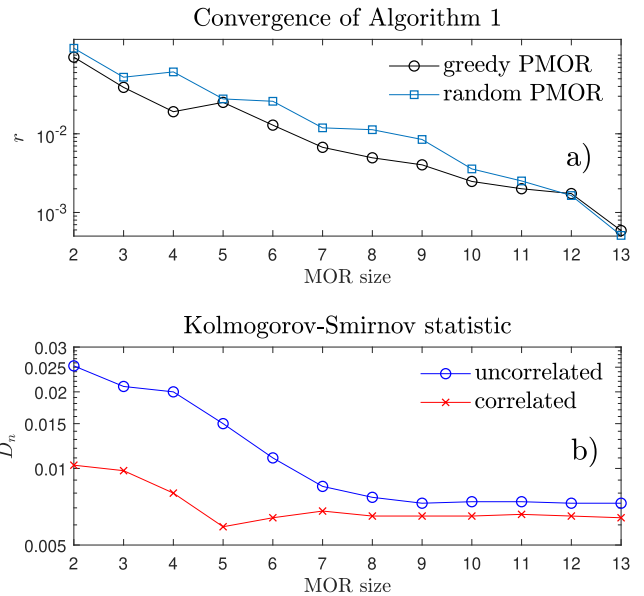
Fig. 5 (*b*) shows the value of the Kolmogorov–Smirnov statistic D_n [54], which is a measure of the *distance* between the two empirical distribution functions obtained using the analytical solution and the (random–based) PMOR method. The null hypothesis that the corresponding random samples come from different distributions is always rejected (at 5% significance level), except for $c = 2$.

To quantify the size of the error introduced by the steps of the algorithm, 10 samples $\boldsymbol{\xi}_k$, with $k = 1, \cdots, 10$, for which the value of *w* goes from the minimum to the maximum (with respect to F_{Ref}) are selected. Fig. 6 (*a*) shows the value of w_k (where $k = 1, \cdots, 10$, denotes the extracted sample $\boldsymbol{\xi}_k$) obtained from F_{Ref} (Reference), F_{MC-13} (MOR), and
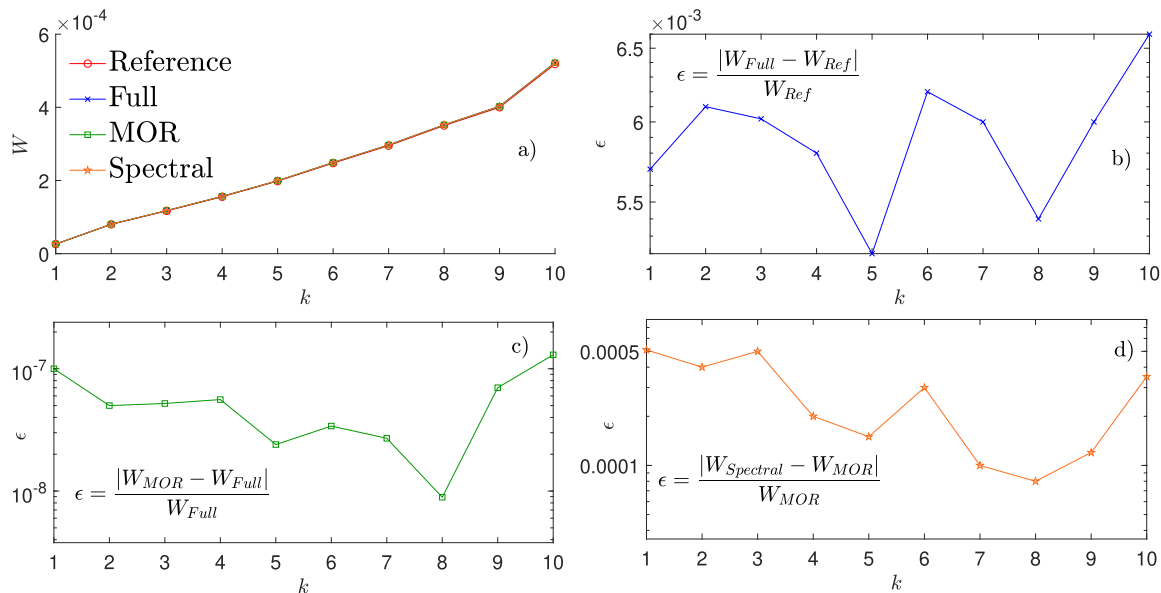
FIGURE 6. Values of w obtained from the MIE, $\mathcal{H}$ Full–VIE, PMOR, and spectral approximation for 10 selected ξ samples (a). Errors introduced by $\mathcal{H}$ Full–VIE (b), PMOR (c), and spectral approximation (d).

TABLE 2. Computational time for the case of the multi–shell sphere.

	Time [s]
Algorithm 1	$\sim 4.1 \cdot 13 + 8 = 61.3$
Algorithm 2	$\sim 23 + 35 = 58$
MC–Spectral, $N_{MC} = 10^6$	~ 28
Total time	144

F_{SP-13} (Spectral) together with the values obtained from the solution of (16) in $\mathcal{H}$–arithmetic (Full–VIE). In the other plots of Fig. 6, the errors introduced by the $\mathcal{H}$–VIE method, PMOR, and the spectral approximations are shown. It can be observed that, even if small, the largest error is introduced by the $\mathcal{H}$–VIE discretization. Instead, the PMOR and the spectral approximation generate errors of orders of magnitude smaller than the $\mathcal{H}$ full–VIE one. The VIE model of the multi–shell sphere consists of 12,960 DoFs. Thus, the storage of the full (uncompressed) parametric VIE system would require ~ 2.7 GB. Instead, thanks to the use of $\mathcal{H}$LIBPro library, the compressed system requires ~ 0.86 GB (i.e. 32% compression ratio) introducing a maximum error in the solution less than 1%. It is worth noting that the compression ratio would significantly decrease with the increase of the number of DoFs [16].

In this case study, due to the large number of random variables, the use of a sparse grid χ^* is mandatory. Indeed, because of the curse of dimensionality, the use of a dense Gaussian grid χ with $P = 5$ gauss points would lead to $N_\chi = P^Q = 5^{10} = 9,765,625$ grid points, resulting in a prohibitive computation time. Instead, for Algorithm 2, a sparse grid χ^* with *only* $N_{\chi^*} = 8,761$ grid points was used. In Table 2, the computation time required by the different steps of the method are reported for the case $c = 13$ and $N_{MC} = 10^6$.
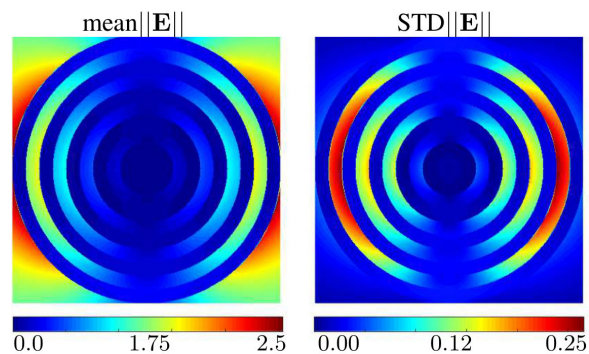

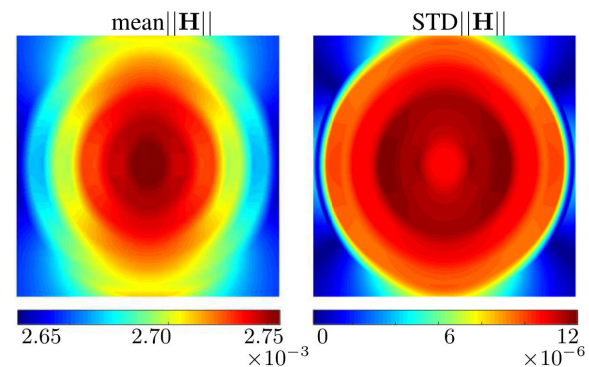**FIGURE 7.** Mean and standard deviation of the electric in [V/m].

FIGURE 8. Mean and standard deviation of the magnetic field magnitude [A/m].

Table 2 shows that the major computational effort is due to the solution of (16), which is solved for 13 selected choices of ξ during Algorithm 1 by means of an $\mathcal{H}$–LU preconditioned GMRES solver [55] which requires ~ 4.1 s. The
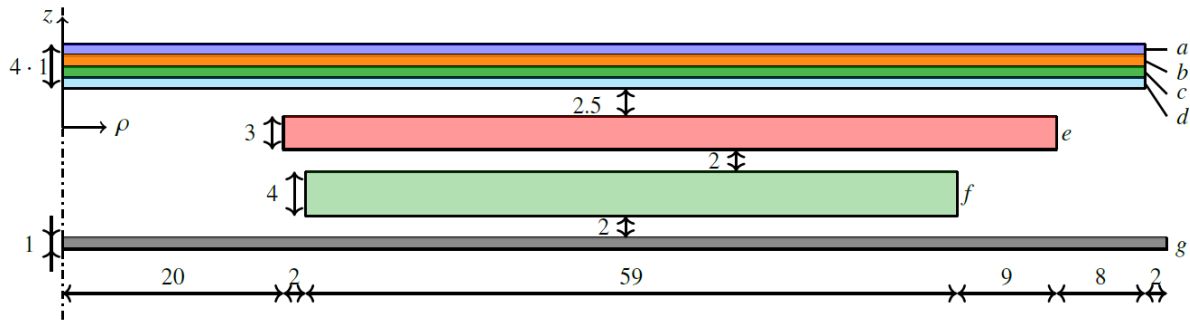
FIGURE 9. Axisymmetric VIE model of the induction cookware. Dimensions are in mm. *a)* Stainless Steel (1), *b)* Aluminum (pot), *c)* Magnetic Steel, *d)* Stainless Steel (2), *e)* External coil, *f)* Ferrite (flux concentrator), *g)* Aluminum (shield).

remaining part of the computation time is mostly due to the (relatively) high dimensionality of the problem, which requires a (relatively) large amount of grid points with Algorithm 2. The timings required to generate F_{MC-13} and F_{SP-13} (consisting of $N_{MC} = 10,000$ samples) are instead ~ 19 s and ~ 0.27 s, respectively. It is noticeable that the spectral approximation drastically reduces the time required by the stochastic analysis with respect to the direct application of MC to $\mathcal{M}_{13}$. Moreover, this gain further increases when N_{MC} grows (i.e. when an higher accuracy is required), and the same spectral approximation can be used with different choices of the PDF and correlation of the parameters. For the sake of comparison, the time required by the direct application of a (non–parallelized) MC method on (16) in $\mathcal{H}$–arithmetic would require $\sim 4.1 \cdot 10,000 = 41,000$ s, whereas, in usual arithmetic (uncompressed case) $\sim 140 \cdot 10,000 = 140,000$ s would have been required. The time required for the generation of F_{Ref} (MC with 10,000 on the Mie solution) is ~ 272 s. ACAplus method has been adopted for the low–rank compression, whereas the compression tolerance is set equal to 10^{-6}, the tolerance for $\mathcal{H}$–LU is 10^{-5} and admissibility value is equal to 2 (see [16] for more details concerning these parameters).

Finally, the proposed algorithm can be adopted also for the evaluation of stochastic information related to the EM fields in the whole 3–D space. Fig. 7 and Fig. 8 show the mean and the standard deviation of the electric and magnetic field magnitude in the $z = 0$ plane obtained as post–processing from the Stochastic–PMOR–VIE algorithm.

B. INDUCTION COOKWARE

As a more applicative test case, uncertainty quantification in the induction cookware presented in [29] is considered.

In this kind of application the power electronic supply consists of ac/dc rectifier, a bus filter, and a resonant inverter. In resonant inverters zero–voltage or zero–current switching are attained when the R–L–C circuit, representing the induction system and the matching capacitance, is resonating. In this condition, power switching losses are minimized enabling high frequency operations, with limited size and cost of the device. In this framework, the analysis of the

TABLE 3. Material parameters of the induction cookware.

	σ_c [MS/m]	μ_r
a	1.04 ± 0.33	1
b	29.1 ± 9.36	1
c	0	$400 \pm 100 - i(175 \pm 43.75)$
d	1.04 ± 0.33	1
e	0	1
f	0	2300 ± 575
g	29.1 ± 9.36	1

equivalent impedance of the coupled inductor-vessel system becomes mandatory in order to obtain an optimal design of its supply system as discussed in [29]. Therefore, the proposed Stochastic–PMOR–VIE method can been adopted to investigate the effects of the uncertainties of the material parameters on the value of the equivalent impedance.

In order to exploit the axial–symmetry of the EM problem, a 3–D VIE model of the induction cookware has been first created. Problem unknowns have been then constrained by using the axial–symmetry condition in order to reduce the number of DoFs of the problem. The geometry of the problem is completely described by Fig. 9 where layers *a*, *b*, *c*, and *d* constitute the bottom part of the pot, layer *e* is the external current–driven coil (the problem excitation), *f* is the magnetic flux concentrator, and *g* is the shield. In Table 3, the material parameters of the various parts of the device are given with their uncertainties. The maximum values of the conductivities are that ones given in [29], whereas the minimum values are chosen assuming that the temperature (which can reach different values in the various parts of the device) attains the maximum value of 230°C. The average value of the permeability is again that one in [29] and a 25% uncertainty is assumed (consistent with most of the data sheets provided by ferromagnetic producers).

Thus, for this case, the number of parameters is $Q = 7$ and the uncertain material quantities of Table 3 are considered as 7 aleatory variables. The same uniform marginal PDFs are assumed for any aleatory variable and a Gaussian copula with correlation matrix $\mathcal{C}$ is introduced [52]. $\mathcal{C}$ has non–zero off–diagonal entries equal to 0.5 for the 5 parameters which model the uncertainties of materials *a*, *b*, *c*, and *d* indicated
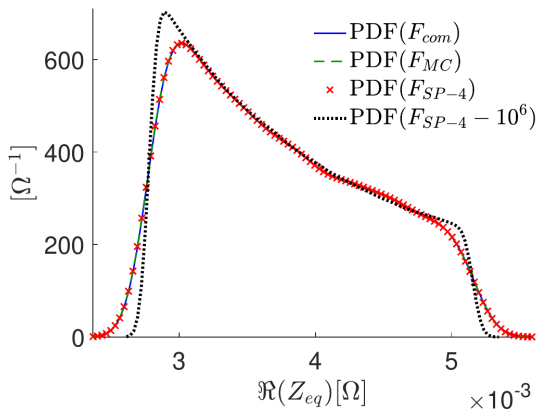
FIGURE 10. Real part of the PDF of $w = Z_{eq}$ obtained from F_{com}, F_{MC}, F_{SP-4}, and $F_{SP-4} - 10^6$.
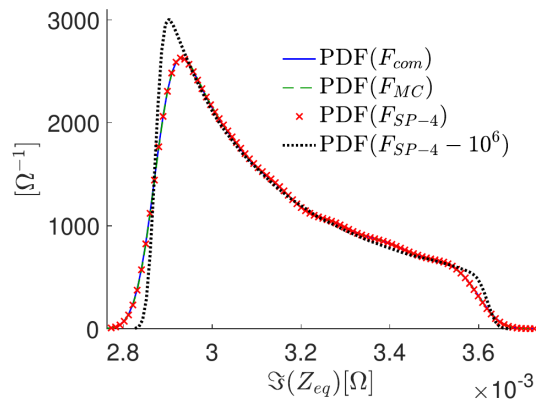

FIGURE 11. Imaginary part of the PDF of $w = Z_{eq}$ obtained from F_{com}, F_{MC}, F_{SP-4}, and $F_{SP-4} - 10^6$.

in Fig. 9, therefore modeling the correlation due to the temperature.

The frequency of the problem is set to 20 kHz and the extracted quantity of interest is the equivalent impedance $w(\xi) = Z_{eq}(\xi)$ of the device at the coil terminals. An uniform (external) current flows in the external coil. Different sets of random samples of $w(\xi)$ are extracted from the Stochastic–PMOR–VIE algorithm. Unlike the case of the sphere, for this case the dimension of the reduced order model obtained from Algorithm 1 is kept constant and equal to $c = 7$ with a final residual of $r = 1.82 \cdot 10^{-4}$. Then, F_{MC} is obtained by directly applying the MC method on the reduced order model $\mathcal{M}_7$. Instead, sets F_{SP-s} are obtained by running an MC method on (25), i.e. the spectral approximation (25) of order $s = 2, \cdots, 6$. Moreover, with the aim of comparing the results obtained from the Stochastic–PMOR–VIE algorithm with a different method, the set of random samples F_{com} is obtained by applying MC on an axisymmetric FEM simulation performed with the COMSOL® commercial software. All the sets described above have been generated from the same set of $N_{MC} = 10,000$ samples ξ. Also for this case, ACAplus method has been adopted for the low–rank compression, whereas the compression tolerance is set equal to 10^{-3}, the tolerance for $\mathcal{H}$–LU is 10^{-2} and admissibility value is equal to 2.

Fig. 10 and Fig. 11 show the PDFs of the real and imaginary parts of $w = Z_{eq}$ obtained from F_{MC}, F_{SP-4}, and F_{com}. Moreover, the PDFs obtained by running MC on the spectral approximation of order 4 with a different set of (correlated) random samples consisting of $N_{MC} = 10^6$ is also shown and indicated as $F_{SP-4} - 10^6$. As can been seen, the three PDFs obtained from F_{MC}, F_{SP-4}, and F_{com} show excellent agreements. Instead, the more accurate PDF obtained from $F_{SP-4} - 10^6$ is quite detached from the others. This shows that when high accuracy is required the MC analysis should be performed with a large amount of samples. As a further remark, this high level of accuracy (i.e. large amount of MC samples) is actually achievable with the proposed algorithm, whereas the application of other traditional approaches would easily result in a prohibitive computation time.
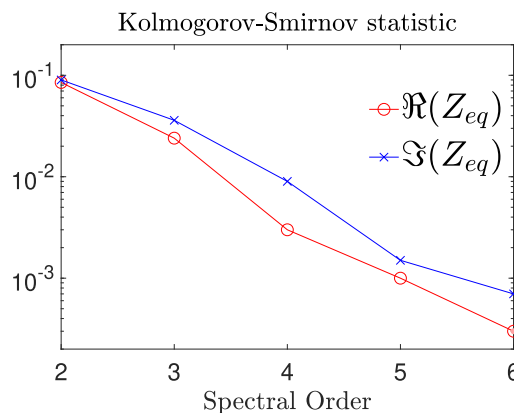

FIGURE 12. Kolmogorov–Smirnov statistic between F_{SP-s}, with $s = 2, \ldots, 6$, and F_{com}.

TABLE 4. Computational time for the case of the induction cookware.

	Time [s]
Algorithm 1	$\sim 7 \cdot 1 + 4.3 = 11.3$
Algorithm 2	$\sim 88.4 + 2.2 = 90.6$
MC–Spectral, $N_{MC} = 10^6$	~ 18
Total time	120

Fig. 12 shows the Kolmogorov–Smirnov statistic, D_n, between the sets F_{SP-s}, with $s = 2, \cdots, 6$, and F_{com}. Numerical results show an exponential convergence of the adopted spectral approximation.

In Table 4 the computation time required by the different steps of the algorithm is reported for the case $s = 5$. For the sake of comparison, the timings required for the generation of F_{com} and F_{MC} (consisting of 10,000 samples) are $\sim 32,160$ s and ~ 359.0 s, respectively. Instead, the time required for the generation of F_{SP-4} ($N_{MC} = 10,000$) is only ~ 0.17 s. Likewise the multi–shell sphere, to alleviate the problem of the curse of dimensionality in Algorithm 2 a sparse grid of $N_{\chi^*} = 2,437$ points was adopted.

The axisymmetric VIE model of the induction cookware consists of 10,328 DoFs. Thus, the storage of the full parametric uncompressed VIE system would require ~ 1.7 GB.

Instead, thanks to the use of $\mathcal{H}$LIBPro library the compressed system only requires 145 MB (i.e. 8.9 % of the uncompressed one). Thanks to the axisymmetric kernel, smoother than the 3–D one, a low compression ratio is attained in this test case. Moreover, $\mathcal{H}$LIBPro library allows for reducing the computation time for the solution of (16) from 8.6 s (time needed for the solution of the uncompressed case) to 1 s, solved with a $\mathcal{H}$–LU preconditioned GMRES.

V. CONCLUSIONS

A Parametric Model Order Reduction (PMOR) technique combined with a spectral approximation approach has been successfully applied to a Volume Integral Equation (VIE) method for uncertainty quantification analyses. 3–D and axisymmetric electromagnetic problems involving conductive, dielectric, and magnetic media can be considered. The electromagnetic media can exhibit complex material properties, whose real and imaginary parts can be considered as independent random parameters.

The computational cost and the memory requirement of the whole Stochastic–PMOR–VIE algorithm is headed by the solution of *only few* deterministic problems and a *low–rank* approximation technique based on $\mathcal{H}$–arithmetic is adopted to further reduce the overall computational effort. The adoption of a random–based PMOR algorithm allows for avoiding the problem of the curse of dimensionality during the construction of the reduced order model without loosing accuracy. Moreover, sparse grids leads to a significant speed–up in the interpolation for the spectral expansion. Thus, the problem of the curse of dimensionality is alleviated and, with respect to original algorithm proposed in [17], a significantly higher amount of random parameters of the order of several tens can be considered.

The proposed technique allows for both uncorrelated and correlated problems. Moreover, the final spectral approximation can be applied *as is* assuming different kinds of probability distributions and correlations between the random materials, without running the algorithm again.

Test cases demonstrate the accuracy and the efficiency of the Stochastic–PMOR–VIE algorithm showing that a very small dimension of the reduced order model is sufficient to attain very high accuracy. In this regard, the comparison between the numerical results of this paper and [17] suggest that the application of PMOR to VIE methods leads to a reduced order model of much smaller dimension with respect the one obtained from PMOR applied to differential methods. Moreover, the exponential convergence of the spectral approximation is observed in the numerical cases and the errors introduced by the PMOR and the spectral approximation are smaller than that ones introduced by the $\mathcal{H}$–VIE discretization. The proposed approach is thus suitable for the study of electromagnetic devices surrounded by large air domains and/or with small air gaps.

With the aim of increasing the industrial applicability of the proposed approach, future researches will investigate the performances of the implemented stochastic code in the case of high frequency problems. Moreover, other compression techniques based, e.g., on the Quantized Tensor Train approach (which has already been efficiently applied to very regular geometries and kernels such as the Boundary Element Methods, but not yet to VIE method) will be the matter of future researches.

REFERENCES

[1] R. Trinchero, M. Larbi, H. Torun, F. G. Canavero, and M. Swaminathan, "Machine learning and uncertainty quantification for surrogate models of integrated devices with a large number of parameters," *IEEE Access*, vol. 7, pp. 4056–4066, 2018.

[2] M. Larbi, I. S. Stievano, F. Canavero, and P. Besnier, "Identfication of main factors of uncertainty in a microstrip line network," *Prog. Electromagn. Res.*, vol. 162, pp. 61–72, 2018. [Online]. Available: http://www.jpier.org/PIER/pier.php?paper=18040607, doi: 10.2528/PIER18040607.

[3] J. P. Eberhard, D. Popović, and G. Wittum, "Numerical upscaling for the eddy-current model with stochastic magnetic materials," *J. Comput. Phys.*, vol. 227, no. 8, pp. 4244–4259, 2008.

[4] K. Wu and J. Li, "A surrogate accelerated multicanonical Monte Carlo method for uncertainty quantification," *J. Comput. Phys.*, vol. 321, pp. 1098–1109, Sep. 2016.

[5] D. Xiu, "Efficient collocational approach for parametric uncertainty analysis," *Commun. Comput. Phys.*, vol. 2, no. 2, pp. 293–309, Apr. 2007.

[6] Q. Su and K. Strunz, "Stochastic circuit modelling with Hermite polynomial chaos," *Electron. Lett.*, vol. 41, no. 21, pp. 1163–1165, Oct. 2005.

[7] D. Xiu, *Numerical Methods for Stochastic Computations: A Spectral Method Approach*. Princeton, NJ, USA: Princeton Univ. Press, 2010.

[8] D. Xiu and G. E. Karniadakis, "The Wiener–Askey polynomial chaos for stochastic differential equations," *SIAM J. Sci. Comput.*, vol. 24, no. 2, pp. 619–644, Jul. 2002.

[9] L. Codecasa and L. Di Rienzo, "Stochastic finite integration technique for magnetostatic problems," *Int. J. Numer. Model., Electron. Netw., Devices Fields*, vol. 30, no. 6, Nov./Dec. 2017, Art. no. e2209.

[10] L. Codecasa and L. Di Rienzo, "Stochastic finite integration technique for eddy-current problems," *IEEE Trans. Magn.*, vol. 51, no. 3, Mar. 2015, Art. no. 7200204.

[11] L. Codecasa and L. Di Rienzo, "Stochastic finite integration technique formulation for electrokinetics," *IEEE Trans. Magn.*, vol. 50, no. 2, Feb. 2014, Art. no. 7014104.

[12] R. Torchio, L. Di Rienzo, and L. Codecasa, "Stochastic PEEC method based on polynomial chaos expansion," *IEEE Trans. Magn.*, vol. 55, no. 6, Jun. 2019, Art. no. 7204504.

[13] P. Ylä-Oijala, M. Taskinen, and J. Sarvas, "Surface integral equation method for general composite metallic and dielectric structures with junctions," *Progr. Electromagn. Res.*, vol. 52, pp. 81–108, Jan. 2005.

[14] R. Torchio, F. Moro, G. Meunier, J.-M. Guichon, and O. Chadebec, "An extension of unstructured-PEEC method to magnetic media," *IEEE Trans. Magn.*, vol. 55, no. 6, Jun. 2019, Art. no. 7200404.

[15] A. Ruehli, G. Antonini, and L. Jiang, *Circuit Oriented Electromagnetic Modeling Using the PEEC Techniques*. Hoboken, NJ, USA: Wiley, 2017.

[16] D. Voltolina, P. Bettini, P. Alotto, F. Moro, and R. Torchio, "High-performance PEEC analysis of electromagnetic scatterers," *IEEE Trans. Magn.*, vol. 55, no. 6, Jun. 2019, Art. no. 7201204.

[17] L. Codecasa and L. Di Rienzo, "MOR-based approach to uncertainty quantification in electrokinetics with correlated random material parameters," *IEEE Trans. Magn.*, vol. 53, no. 6, Jun. 2017, Art. no. 8201204.

[18] G. Rozza, D. B. P. Huynh, and A. T. Patera, "Reduced basis approximation and a posteriori error estimation for affinely parametrized elliptic coercive partial differential equations," *Arch. Comput. Methods Eng.*, vol. 15, no. 3, pp. 1, 2008.

[19] P. Benner, S. Gugercin, and K. Willcox, "A survey of projection-based model reduction methods for parametric dynamical systems," *SIAM Rev.*, vol. 57, no. 4, pp. 483–531, 2019.

[20] M. M. Botha, "Solving the volume integral equations of electromagnetic scattering," *J. Comput. Phys.*, vol. 218, no. 1, pp. 141–158, 2006.

[21] L. Rahmouni, R. Mitharwal, and F. P. Andriulli, "Two volume integral equations for the inhomogeneous and anisotropic forward problem in electroencephalography," *J. Comput. Phys.*, vol. 348, pp. 732–743, Nov. 2017.

[22] R. Kriemann. *H-Lib^{Pro} (v2.7.1)*. Accessed: Feb. 18, 2019. [Online]. Available: http://www.hlibpro.com

[23] S. Börm, L. Grasedyck, and W. Hackbusch, "Introduction to hierarchical matrices with applications," *Eng. Anal. Boundary Elements*, vol. 27, no. 5, pp. 405–422, May 2003.

[24] K. Zhao, M. N. Vouvakis, and J.-F. Lee, "The adaptive cross approximation algorithm for accelerated method of moments computations of EMC problems," *IEEE Trans. Electromagn. Compat.*, vol. 47, no. 4, pp. 763–773, Nov. 2005.

[25] J. Markkanen, P. Yla-Oijala, and A. Sihvola, "Discretization of volume integral equation formulations for extremely anisotropic materials," *IEEE Trans. Antennas Propag.*, vol. 60, no. 11, pp. 5195–5202, Nov. 2012.

[26] J. Markkanen, C.-C. Lu, X. Cao, and P. Yla-Oijala, "Analysis of volume integral equation formulations for scattering by high-contrast penetrable objects," *IEEE Trans. Antennas Propag.*, vol. 60, no. 5, pp. 2367–2374, May 2012.

[27] A. Sommer, O. Farle, and R. Dyczij-Edlinger, "A new method for accurate and efficient residual computation in adaptive model-order reduction," *IEEE Trans. Magn.*, vol. 51, no. 3, Mar. 2015, Art. no. 1100104.

[28] R. Torchio, "A volume PEEC formulation based on the cell method for electromagnetic problems from low to high frequency," *IEEE Trans. Antennas Propag.*, to be published, doi: 10.1109/TAP.2019.2927789.

[29] F. Moro, P. Alotto, M. Guarnieri, and A. Stella, "Impedance design of cooking appliances with multilayer induction-efficient cookware," in *Proc. 39th Annu. Conf. IEEE Ind. Electron. Soc.*, Vienna, Austria, Nov. 2013, pp. 5040–5045.

[30] P. Yla-Oijala, J. Markkanen, S. Jarvenpaa, and S. P. Kiminki, "Surface and volume integral equation methods for time-harmonic solutions of Maxwell's equations (invited paper)," *Prog. Electromagn. Res.*, vol. 149, pp. 15–44, 2014. [Online]. Available: http://www.jpier.org/PIER/pier.php?paper=14070105, doi: 10.2528/PIER14070105.

[31] R. Torchio, P. Alotto, P. Bettini, D. Voltolina, and F. Moro, "A 3-D PEEC formulation based on the cell method for full-wave analyses with conductive, dielectric, and magnetic media," *IEEE Trans. Magn.*, vol. 54, no. 3, Mar. 2018, Art. no. 7201204.

[32] F. P. Andriulli, "Loop-star and loop-tree decompositions: Analysis and efficient algorithms," *IEEE Trans. Antennas Propag.*, vol. 60, no. 5, pp. 2347–2356, May 2012.

[33] S. B. Adrian, F. P. Andriulli, and T. F. Eibert, "On a refinement-free Calderón multiplicative preconditioner for the electric field integral equation," *J. Comput. Phys.*, vol. 376, pp. 1232–1252, Jan. 2019.

[34] M. Li and W. C. Chew, "Applying divergence-free condition in solving the volume integral equation," *Prog. Electromagn. Res.*, vol. 57, pp. 311–333, 2006. [Online]. Available: http://www.jpier.org/PIER/pier.php?paper=0506133, doi: 10.2528/PIER05061303.

[35] G. Rubinacci, S. Ventre, F. Villone, and Y. Liu, "A fast technique applied to the analysis of resistive wall modes with 3D conducting structures," *J. Comput. Phys.*, vol. 228, no. 5, pp. 1562–1572, 2009.

[36] R. Torchio, P. Bettini, and P. Alotto, "PEEC-based analysis of complex fusion magnets during fast voltage transients with H-matrix compression," *IEEE Trans. Magn.*, vol. 53, no. 6, Jun. 2017, Art. no. 7200904.

[37] C. Geoga. *KernelMatrices.Jl*. Accessed: Oct. 4, 2019. [Online]. Available: https://bitbucket.org/cgeoga/kernelmatrices.jl/src/master/

[38] S. Massei, D. Palitta, and L. Robol. *HM-Toolbox*. Accessed: Oct. 4, 2019. [Online]. Available: https://github.com/numpi/hm-toolbox

[39] S. Massei, D. Palitta, and L. Robol, "Solving rank-structured Sylvester and Lyapunov equations," *SIAM J. Matrix Anal. Appl.*, vol. 39, no. 4, pp. 1564–1590, 2018.

[40] F. H. Rouet. *STRUMPACK (v.1.1.1)*. Accessed: Nov. 1, 2017. [Online]. Available: http://portal.nersc.gov/project/sparse/strumpack/

[41] F. H. Rouet, X. S. Li, P. Ghysels, and A. Napov, "A distributed-memory package for dense hierarchically semi-separable matrix computations using randomization," *ACM Trans. Math. Softw.*, vol. 42, no. 4, 2016, Art. no. 27.

[42] D. Kressner, S. Massei, and L. Robol, "Low-rank updates and a divide-and-conquer method for linear matrix equations," *SIAM J. Sci. Comput.*, vol. 41, no. 2, pp. A848–A876, 2019.

[43] J. Xia, S. Chandrasekaran, M. Gu, and X. S. Li, "Fast algorithms for hierarchically semiseparable matrices," *Numer. Linear Algebra Appl.*, vol. 17, pp. 953–976, Dec. 2010.

[44] K. L. Ho. *FLAM: Fast Linear Algebra in MATLAB*. Accessed: Oct. 4, 2019. [Online]. Available: https://github.com/klho/FLAM, doi: 10.5281/zenodo.1253582.

[45] R. Baptista, V. Stolbunov, and P. B. Nair, "Some greedy algorithms for sparse polynomial chaos expansions," *J. Comput. Phys.*, vol. 387, pp. 303–325, Jun. 2019.

[46] Z. Fei, Y. Huang, J. Zhou, and C. Song, "Numerical analysis of a transmission line illuminated by a random plane-wave field using stochastic reduced order models," *IEEE Access*, vol. 5, pp. 8741–8751, 2017.

[47] Y. Yue, L. Feng, P. Meuris, W. Schoenmaker, and P. Benner, "Application of Krylov-type parametric model order reduction in efficient uncertainty quantification of electro-thermal circuit models," in *Proc. Prog. Electromagn. Res. Symp. (PIERS)*, 2015, pp. 379–384.

[48] R. Pulch, "Model order reduction for stochastic expansions of electric circuits," in *Scientific Computing in Electrical Engineering* (Polymers of Hexadromicon), vol. 3, J. Peters, Ed. Cham, Switzerland: Springer, 2016, pp. 223–231.

[49] P. Chen, A. Quarteroni, and G. Rozza, "Model order reduction techniques for uncertainty quantification problems," Ph.D. dissertation, École Polytechn. Fédérale De Lausanne, Lausanne, Switzerland, 2014.

[50] G. Winckel. *SPARSE_GRI_HW MATLAB Library*. Accessed: Oct. 4, 2019. [Online]. Available: https://people.sc.fsu.edu/~jburkardt/m_src/sparse_grid_hw/sparse_grid_hw.html

[51] L. M. M. van den Bos, B. Koren, and R. P. Dwight, "Non-intrusive uncertainty quantification using reduced cubature rules," *J. Comput. Phys.*, vol. 332, pp. 418–445, Mar. 2017.

[52] R. B. Nelsen, *An Introduction to Copulas*. New York, NY, USA: Springer, 1999.

[53] J. Schäfer. *MatScat MATLAB Tool*. Accessed: Oct. 4, 2019. [Online]. Available: https://it.mathworks.com/matlabcentral/fileexchange/36831-matscat

[54] F. J. Massey, Jr., "The Kolmogorov–Smirnov test for goodness of fit," *J. Amer. Stat. Assoc.*, vol. 46, no. 253, pp. 68–78, 1951.

[55] S. Le Borne and R. Kriemann, "H-FAINV: Hierarchically factored approximate inverse preconditioners," *Comput. Vis. Sci.*, vol. 17, no. 3, pp. 135–150, 2015.

RICCARDO TORCHIO was born in Padova, Italy, in 1992. He received the M.S. degree in electrical engineering from the University of Padova, Padova, in 2016. He is currently pursuing the Ph.D. degree (joint–Ph.D.) in electrical engineering with the University of Padova, Italy, and the Grenoble Electrical Engineering Laboratory (G2ELab), France. His research interests include numerical methods, low-rank compression techniques, uncertainty quantifications, and the development of integral formulations for the study of low and high frequency electromagnetic devices.

LORENZO CODECASA received the Ph.D. degree in electronic engineering from the Politecnico di Milano, in 2001.

From 2002 to 2010, he was an Assistant Professor of electrical engineering with the Department of Electronics, Information, and Bioengineering, Politecnico di Milano, where he has been an Associate Professor of electrical engineering, since 2010. His main research contributions are in theoretical analysis and in computational investigation of electric circuits and electromagnetic fields. In his research on heat transfer and thermal management of electronic components, he has introduced original industrial-strength approaches to the extraction of compact thermal models, currently available in commercial software. In his research areas, he has authored or coauthored over 190 articles in refereed international journals and conference proceedings. For these activities, he received the Harvey Rosten Award for Excellence, in 2016. In 2019, he served as the Program Chair for the conference Thermal Investigation of Integrated Circuits (THERMINIC). He has been serving as an Associate Editor for the IEEE Transactions on Components, Packaging, and Manufacturing Technology.

LUCA DI RIENZO (SM'12) received the Laurea (M.Sc.) *(cum laude)* and Ph.D. degrees in electrical engineering from the Politecnico di Milano, in 1996 and 2001, respectively. He is currently an Associate Professor with the Dipartimento di Elettronica, Informazione e Bioingegneria at Politecnico di Milano. His current research interests are in the field of computational electromagnetics and include magnetic inverse problems, integral equation methods, surface impedance boundary conditions, and uncertainty quantification. He is an Associate Editor-in-Chief of *The Applied Computational Electromagnetics Society Journal* and of *COMPEL-The International Journal for Computation and Mathematics in Electrical and Electronic Engineering* and a member of the Editorial Board of *Sensing and Imaging*.

FEDERICO MORO received the M.S. degree in electrical engineering, the Ph.D. degree in bio-electromagnetic and electromagnetic compatibility, and the B.S. degree in mathematics from the University of Padova, Italy, in 2003, 2007, and 2012, respectively. From January 2005 to July 2005, he was a Visiting Researcher with the Department of Physics, Swansea University, U.K. From 2007 to 2010, he was a Research Associate with the Department of Electrical Engineering, University of Padova, where he has been an Assistant Professor of electrical engineering at the Department of Industrial Engineering, since 2010. He is author of more than 100 articles in peer-reviewed international journals and conference proceedings. His research interests include numerical methods for computing electromagnetic field problems and numerical modeling of multiphysics and multiscale problems.

● ● ●